1	Thin-film Composite Membranes Based on Hyperbranched Poly(ethylene oxide) for
2	CO ₂ /N ₂ Separation
3	
4	Gengyi Zhang, ¹ Thien N. Tran, ¹ Liang Huang, ¹ Erda Deng, ¹ Adrienne Blevins, ² Wenji Guo, ¹
5	Yifu Ding, ² and Haiqing Lin* ¹
6	
7	
8	¹ Department of Chemical and Biological Engineering, University at Buffalo, The State
9	University at New York, Buffalo, New York 14260, USA
10	² Membrane Science, Engineering and Technology (MAST) Center, Paul M. Rady Mechanica
11	Engineering, University of Colorado at Boulder, Boulder, CO 80309, USA
12	
13	Corresponding author: E-mail: haiqingl@buffalo.edu
14	
15	
16	
17	
18	Prepared for submission to Journal of Membrane Science
19	

ABSTRACT

Cross-linked amorphous poly(ethylene oxide) (XLPEO) is one of the leading membrane materials for post-combustion CO₂ capture. For example, XLPEO prepared from poly(ethylene glycol) methyl ether acrylate (PEGMEA) exhibited CO₂ permeability of 570 Barrer and CO₂/N₂ selectivity of 41 at 35°C. However, these XLPEOs cannot be dissolved in coating solutions, making it impossible to be fabricated into thin-film composite (TFC) membranes using state-of-the-art manufacturing processes. In this study, we synthesized high molecular weight yet soluble HPEO via atom transfer radical polymerization (ATRP). These polymers were thoroughly characterized and compared with XLPEO, including thermal transitions, free volumes, and puregas sorption and permeation properties. A polymer with the best combination of CO₂ permeability (540 Barrer) and CO₂/N₂ selectivity (43) was fabricated into defect-free TFC membranes with a thickness as thin as 506 ± 44 nm. When challenged with simulated flue gas containing water vapor at 35°C for over 100 h, the membrane shows stable CO₂ permeance of 850 GPU and CO₂/N₂ selectivity of 37, comparable to the leading commercial membranes for carbon capture.

KEYWORDS: Poly(ethylene oxide); CO₂/N₂ separation; thin-film composite membrane; post-combustion carbon capture; atom transfer radical polymerization

1. Introduction

Carbon capture for utilization and sequestration is an essential path to mitigate the CO₂ emissions to the atmosphere if fossil fuels remain as major sources for electricity generation. The flue gas has an enormous volume and very low CO₂ partial pressure (0.04 – 0.13 atm), making the capture a very challenging proposition [1, 2]. Membrane technology has become one of the leading technologies for CO₂ capture because of its high energy efficiency, low maintenance, and small footprint [3-8]. In particular, industrial membranes with CO₂ permeance of >1000 GPU (1 GPU = 10⁻⁶ cm³(STP) cm⁻² s⁻¹ cmHg⁻¹) and CO₂/N₂ selectivity of >30 would make the membrane processes economically competitive with the leading amine sorption processes if a multi-step membrane system incorporated with a cryogenic unit for liquid CO₂ production is used [2]. The cost of the CO₂ capture can be further reduced by enhancing the CO₂ permeance but is not influenced by the CO₂/N₂ selectivity once it is above 30.

The first challenge in developing industrial membranes is to design materials possessing excellent CO₂/N₂ separation properties [9, 10]. One of the leading materials is based on poly(ethylene oxide) (PEO) because of the affinity of polar ether oxygens towards CO₂ (generating high CO₂/N₂ solubility selectivity) and good chain flexibility (inducing high CO₂ diffusivity) [6, 11-13]. For instance, a cross-linked PEO (XLPEO) synthesized from a prepolymer solution containing 98.7 mass% poly(ethylene glycol) methyl ether acrylate (PEGMEA, Mn = 480 g/mol) and 1.3 mass% poly(ethylene glycol) diacrylate (PEGDA, Mn = 700 g/mol) exhibited CO₂ permeability of 570 Barrer (1 Barrer = 10⁻¹⁰ cm³(STP) cm cm⁻² s⁻¹ cmHg⁻¹) and CO₂/N₂ selectivity of 41 at 35°C [14]. However, the polymers are cross-linked and cannot be dissolved into a coating solution for fabricating membranes using typical equipment and processes [7, 15].

The second challenge in developing industrial membranes is to form a thin layer (<1 µm) of a highly selective material on a porous support (providing mechanical strength) [7, 16]. Current gas separation membranes are usually prepared from polymer solutions via phase-inversion processes (to form integral asymmetric membranes) or coating processes (to form thin-film composite or TFC membranes). As XLPEOs cannot be processed into industrial membranes, other PEO-based polymers have been widely investigated for TFC membranes, such as Pebax® and PolyActiveTM that are microphase-separated block copolymers containing a continuous rubbery PEO phase and the other continuous glassy polymer phase (such as polyamide for Pebax and polybutylene terephthalate for PolyActive). The glassy polymer phase has much lower gas permeability than the amorphous PEO, and thus, Pebax and PolyActive exhibit CO₂/N₂ selectivity close to the amorphous PEO but excellent solution-coatability to be fabricated into TFC membranes [17-21]. For instance, TFC membranes comprising 125-nm PolyActive displayed CO₂ permeance as high as 1300 GPU and good CO₂/N₂ selectivity of 58 at 20°C [22]. Defect-free XLPEO layers of ~60 nm were also formed by the continuous assembly on top of a gutter layer of polydimethylsiloxane (PDMS), and the resulting membranes exhibited CO₂ permeance of 1200 GPU with mixed-gas CO₂/N₂ selectivity of 22 [23, 24]. By contrast, if the PEGMEA-co-PEGDA (98.7:1.3 by mass ratio) can be fabricated into thin layers of 200 nm, the resulting membranes can have potential CO₂ permeance as high as 2850 GPU at 35°C.

60

61

62

63

64

65

66

67

68

69

70

71

72

73

74

75

76

77

78

79

80

81

82

The key challenge to fabricate PEGMEA-co-PEGDA into TFC membranes is to prepare the polymers with high molecular weight (to achieve good mechanical properties) and good solubility in solvents. Interestingly, PEGDA has been polymerized to produce high molecular weight and soluble polymers using atom transfer radical polymerization (ATRP) because it allows a slow and controllable polymerization rate and thus results in desired molecular weight [25-27].

PEGMEA was polymerized using single-electron transfer living radical polymerization (SET-LRP) [28], and poly(ethylene glycol) monomethyl ether methacrylate (PEGMA) was also synthesized by ATRP [29]. However, these polymers are often explored for drug and gene delivery due to their biocompatibility and low toxicity and have not been utilized for TFC membranes.

Herein, we synthesized high molecular weight and hyperbranched PEO from PEGMEA and PEGDA using ATRP and explored their potential for high-performance TFC membranes for CO_2/N_2 separation. First, the polymers were thoroughly characterized for physical properties, such as density, glass transition temperature (T_g), and free volume, and compared with XLPEO prepared via photopolymerization. Second, pure-gas transport properties of N_2 , H_2 , CH_4 , and CO_2 in these polymers were determined to illustrate the effect of molecular weight on gas separation properties. Third, the polymer with the best separation properties was fabricated into TFC membranes, and the CO_2/N_2 separation properties were determined using pure- and mixed-gas. The membranes were also challenged with simulated flue gas containing water vapor, and their performance is compared with the state-of-the-art membranes to elucidate their potential for carbon capture.

2. Experimental

2.1 Materials

For polymer synthesis, PEGMEA (Mn = 480 g/mol), PEGDA (Mn = 700 g/mol), anhydrous copper(II) bromide (CuBr₂, 99+%), pentaerythritol tetrakis(2-bromo-isobutyrate) (4f-BiB, 97%), anhydrous dimethyl sulfoxide (DMSO), 1-hydroxycyclohexyl phenyl ketone (HCPK), anhydrous tetrahydrofuran (THF) and diethyl ether were acquired from Sigma-Aldrich (St. Louis, MO). Tris[2-(dimethylamino)ethyl]amine (Me₆TREN, 99+%) was procured from Alfa Aesar

(Haverhill, MA). Bare copper wire with a diameter of ≈0.8 mm and hydrochloric acid (HCl) were supplied by ThermoFisher Scientific (Waltham, MA).

For TFC membrane fabrication, polysulfone (PSF) support with a nominal molecular weight cut-off (MWCO) of 30 kDa was purchased from Ultura Inc. (Oceanside, CA). Sylgard 184 (PDMS) was procured from Dow Silicones Corporation (Midland, MI). Hexane, isopropyl alcohol (IPA), and iso-octane were procured from Sigma-Aldrich.

For the characterization of polymers and membranes, DMSO-d₆ was acquired from Sigma-Aldrich. High-pressure gas of CH₄, N₂, H₂, and CO₂ with ultrahigh purity were provided by Airgas, Inc. (Radnor, PA).

2.2 Polymer synthesis and membrane fabrication

Synthesis of high molecular weight PEO via ATRP. A typical procedure to synthesize the high molecular weight PEO is described below [30, 31]. PEGMEA (9.8 g, 19.6 mmol), PEGDA (0.2 g, 0.285 mmol), CuBr₂ (0.0112 g, 0.05 mmol), and 4f-BiB (initiator) were first added into anhydrous DMSO (10 ml) in a flask. The molar ratio of the PEGMEA to the initiator (i.e., r) was varied from 400 to 2000 to obtain polymers with different molecular weights. Second, copper wire (7 cm) was polished by HCl and then added to the mixture with Me₆TREN (62.4 μl). The solution was degassed for at least four freeze-pump-thaw cycles and then transferred to a water bath at 33°C to initiate the polymerization under argon protection. Third, after a 90-min reaction, THF (30 ml) was poured into the flask to stop the reaction, and then the solution was precipitated in diethyl ether (50 ml). Finally, the precipitated polymer was dried using a rotary evaporator to remove the residual solvent and then dissolved in water or acetone for further use. The polymers are named HPEOx-r, where x is the mass percentage of the PEGDA in the monomers (including PEGMEA and PEGDA).

The HPEO films (\sim 300 µm) were prepared via a solution casting method. An acetone solution containing a desirable content of HPEO was cast in a Teflon petri dish and dried at 23°C in the air for 48 h and then under vacuum for 8 h.

Preparation of TFC membranes. The membranes were prepared using a multi-step coating procedure. First, the PSF support was immersed in deionized (DI) water for 30 min with ultrasonication to remove the pore preservers, followed by sequential solvent exchange with IPA for 20 min and iso-octane for 1 h with ultrasonication. The support was then dried in the fume hood for further use.

Second, a PDMS solution was prepared by dissolving PDMS (2 g) and the catalyst (0.2 g) in hexane (2 g) and then polymerized at 60°C for 1 h before the termination by adding cold hexane. The solution was diluted to 10 mass% and kept in a refrigerator before use. The gutter layer was formed by coating a solution containing 3 mass% PDMS on the PSF support using Gardo automatic drawdown machine. After drying with a heat gun for 3 min, the membrane was kept at 60°C for 2 h for the PDMS to fully cross-link. Finally, the HPEO layer was coated using a solution containing various amounts of HPEO in an IPA and water solution (96.5:3.5 by weight). The membrane was dried using the heat gun for 5 min to evaporate the solvents.

Synthesis of XLPEO2. XLPEO2 films were prepared by photopolymerization as the reference material for HPEO2 following a well-established method [14, 32]. DMSO was used to prepare the prepolymer solutions so that the procedure is consistent with the ATRP process. After the polymerization, the films were dried under vacuum at 50°C for 48 h to evaporate the DMSO.

2.3 Determination of chemical and physical structures

¹HNMR (500 MHz Varian Inova-500 spectrometer) was used to determine chemical structure of HPEO. The chemical shift peaks are shown below: ¹H NMR (DMSO-d₆): δ 6.32 (yH,

152 RCOOCH₂CH₂O), 4.08 (8H, CH₂COOCCH₃CH₃), 4.08 (2(x+y+2z)H, RCOOCH₂CH₂O), 3.62 153 (4(x+y+z)H, RCOOCH₂CH₂O), 3.49 ((24x+48(y+z))H, OCH₂CH₂OCH₂CH₂OCH₂CH₂), 3.49

cis CH₂=CH), 6.18 (yH, ROOCCH=CH₂), 5.92 (yH, trans CH₂=CH), 4.19 (2(y)H,

154 (2(x)H, CH₂OCH₃), 3.22 (3(x)H, CH₂OCH₃), 2.42~2.12 ((x+y+z)H, CH₂CH), 1.93~1.30

155 (2(x+y+z)H, CH₂CH), 1.05 (6H, RCOOCCH₃CH₃).

151

156

157

158

159

160

161

162

163

171

172

173

The molecular weight and polydispersity of the HPEO were analyzed using Viscotek Gel Permeation Chromatography (GPC) equipped with a VE-3580 refractive index detector (Malvern Panalytical, UK). VERTEX 70 Fourier transform infrared (FTIR) spectrometer (Billerica, MA) was used at ≈23°C. Differential Scanning Calorimetry (DSC) of Q2000 (TA Instruments, New Castle, DE) was used to determine thermal transitions at temperatures from -90 to 60°C at 20 °C min⁻¹ under N₂ flow. Rigaku Ultima IV (Rigaku Corporation, Tokyo, JP) was used to collect wideangle X-ray diffraction (WAXD) spectra. It scanned from 10° to 80° at 1° min⁻¹, and the *d*-spacing is calculated by Bragg`s equation:

$$164 d = \frac{\lambda}{2sin\theta} (1)$$

where λ is the wavelength of CuK α radiation (1.54 Å), and θ is the diffraction peak.

The film density (ρ_P) was measured by Mettler Toledo XS64 and calculated using Equation 2 [32, 33]:

$$\rho_P = \frac{M_A}{M_A - M_B} \rho_L \tag{2}$$

where M_A is the film mass in the air, M_B is the film mass in decane, and ρ_L represents the decane density (0.73 g/cm³).

A micrometer of Starrett 2900 (L.S. Starrett Co., Athol, MA) was used to measure the film thickness. The films were first sandwiched between two microscope glass slides (150 μ m) to avoid the tip penetration into the soft films (~300 μ m). For the TFC membranes, the thickness of the

HPEO and PDMS layer was determined using F20 Film Measurement Instrument (Filmetrics, San Diego, CA) [34]. The PSF support was first dissolved by dimethylformamide (DMF), and then the PDMS or HPEO/PDMS layer was transferred onto a silicon wafer and dried under vacuum for 2 h before the thickness measurement by F20. The refractive index value was 1.47 for HPEO, 1.43 for PDMS, and 1.63 for PSF [35-37].

A Field Emission Scanning Electron Microscope (FE-SEM) (Hitachi SU70, Tokyo, Japan) was used to obtain the cross-section images of TFC membranes. Gold nanoparticles were coated before the imaging. Atomic Force Microscopy (AFM) was used to determine sample surface roughness and modulus. A Cypher model ES atomic force microscope (Asylum Research, Santa Barbara, CA) was used in fast force mapping (FFM) mode. Roughness measurements were taken from the height channel scans that provided topography maps, and average modulus and adhesion values were taken from the modulus map and adhesion maps, respectively. These scans were conducted under photothermal excitation using a gold-coated FMR tip (Nanosensors, Switzerland). The JKR contact model was used to estimate elastic modulus at each pixel.

2.4 Determination of gas transport properties

A constant-volume and variable-pressure apparatus was used to determine pure-gas permeability (P_A) at a feed pressure of 10 - 30 psig and 35°C [32]. Pure- and mixed-gas permeance of the TFC membranes was determined using a constant-pressure and variable-volume system at 35°C [33, 34]. For the mixed-gas test, gas mixtures were prepared by in-line mixing of pure gases, and the permeate was swept using helium. The composition of gas mixtures was determined using 3000 Micro GC (Inficon Inc., Syracuse, NY). TFC membranes often have an unknown selective layer thickness (I), and thus the mixed-gas permeance for component A (I) can be calculated using Equation 3 [33]:

197
$$\frac{P_A}{l} = \frac{x_A S}{x_{Sweep} A_m(p_{2,A} - p_{1,A})}$$
 (3)

where S represents the sweep gas flow rate, A_m is the membrane area, and x_A and x_{sweep} are the volume fraction of gas A and He in the sweep-out stream, respectively.

A dual-volume and dual-transducer apparatus was used to determine sorption isotherms of CO₂ and C₂H₆ in polymers (\sim 1.39 cm³) according to a pressure decay method [38]. Gas solubility (S_4 , cm³(STP) cm⁻³ atm⁻¹) can be calculated using the following equation [39]:

$$S_A = C_A/p_A \tag{4}$$

where C_A is the concentration of the gas dissolved in the polymer at pressure p_A . Gas diffusion coefficient (D_A) can be calculated according to the solution-diffusion model, as shown in Equation 5:

$$D_A = P_A/S_A \tag{5}$$

3.1 Synthesis and characterization of HPEO

3. Results and discussion

Figure 1a illustrates the synthetic route of the HPEO2 by ATRP and an example ¹H-NMR spectrum for HPEO2-800. The polymer demonstrates a strong chemical shift of ethylene oxide at 3.49 ppm, a chemical shift at 3.22 for methyl groups, and peaks of 6.4 - 5.9 ppm, indicating a small number of unreacted vinyl groups. Other polymers have similar structures, as shown in Figure S1 in the Supporting Information (SI).

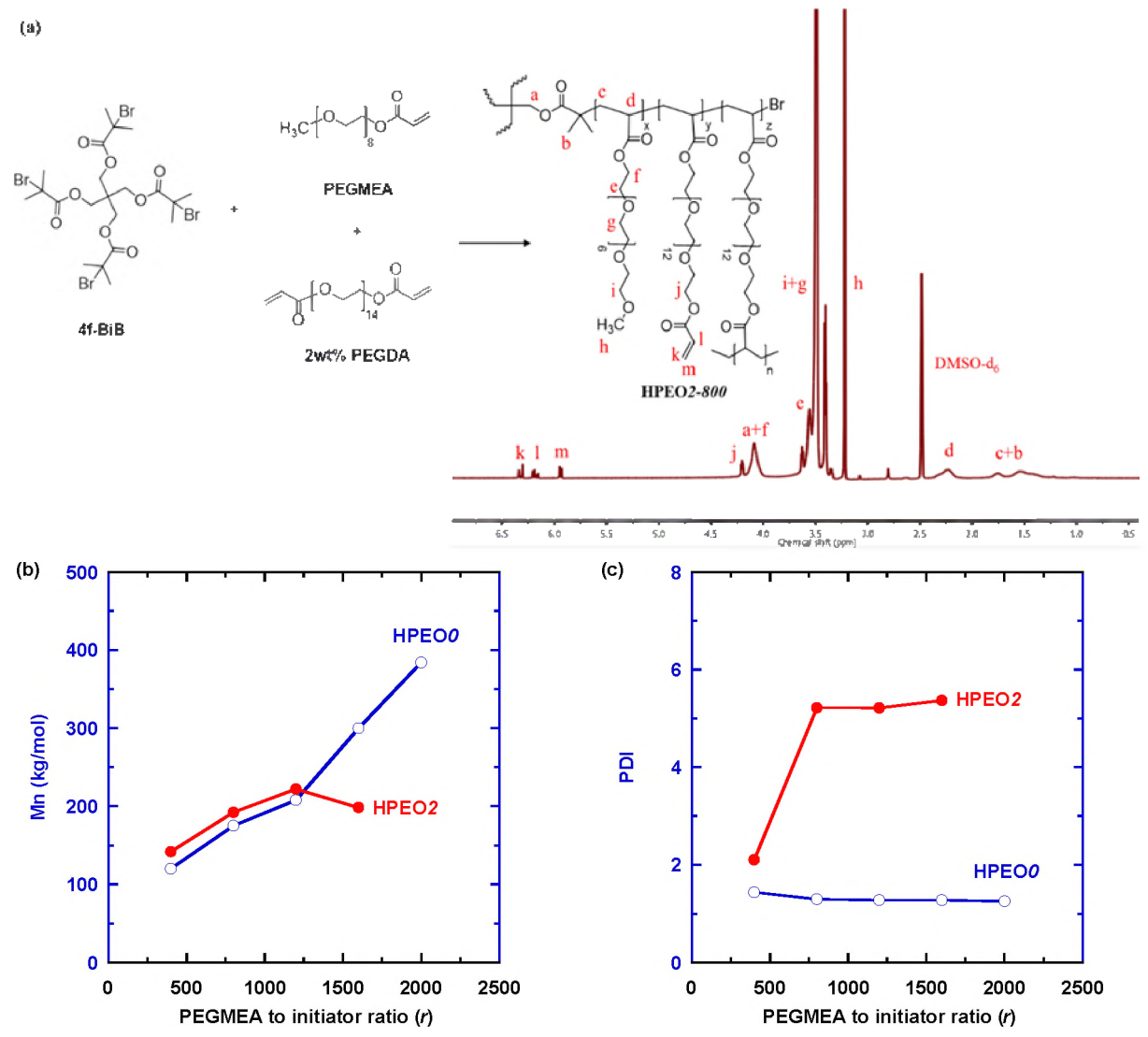


Figure 1. Synthesis and characterization of HPEO θ and HPEO θ . (a) Synthetic route of the HPEO θ via ATRP, and ¹H NMR spectrum of the HPEO θ -80 θ . Effect of the θ (molar ratio of PEGMEA to 4f-BIB) on (b) Mn and (c) PDI for HPEO θ and HPEO θ .

Figure 1b,c compares the molecular weight (Mn) and polydispersity index (PDI) as a function of r in HPEO θ and HPEO2, respectively. For HPEO θ , increasing the r value increases the molecular weight (cf. Table S1), while the PDI remains low at \approx 1.2, confirming the controlled polymerization by ATRP [28]. However, the polymers are too weak to form freestanding films, even for HPEO θ -2000 with the highest Mn (384 kDa). By contrast, introducing 2 mass% PEGDA into the reaction mixture improves the mechanical strength of the polymers to form freestanding

films, while the obtained HPEO2 can still be soluble in solvents. Interestingly, the HPEO2 shows lower Mn values than HPEO θ at the same r values. Increasing the r value significantly increases the PDI for HPEO2, indicating a hyperbranched structure, which is consistent with the literature. For example, hyperbranched PEO prepared from PEGDA via ATRP showed Mw ranging from 45 to 403 kDa and PDI varying from 3.2 to 8.8 [25, 27].

Figure 2a compares the WAXD patterns for XLPEO2 and HPEO samples. The XLPEO2 exhibits a broad halo at 2θ values of 21° , consistent with previous reports [40]. The HPEO samples show diffraction patterns similar to XLPEO2, indicating that they are amorphous at \approx 23°C. All polymers show the same d-spacing value (4.2 Å, as recorded in Table 1).



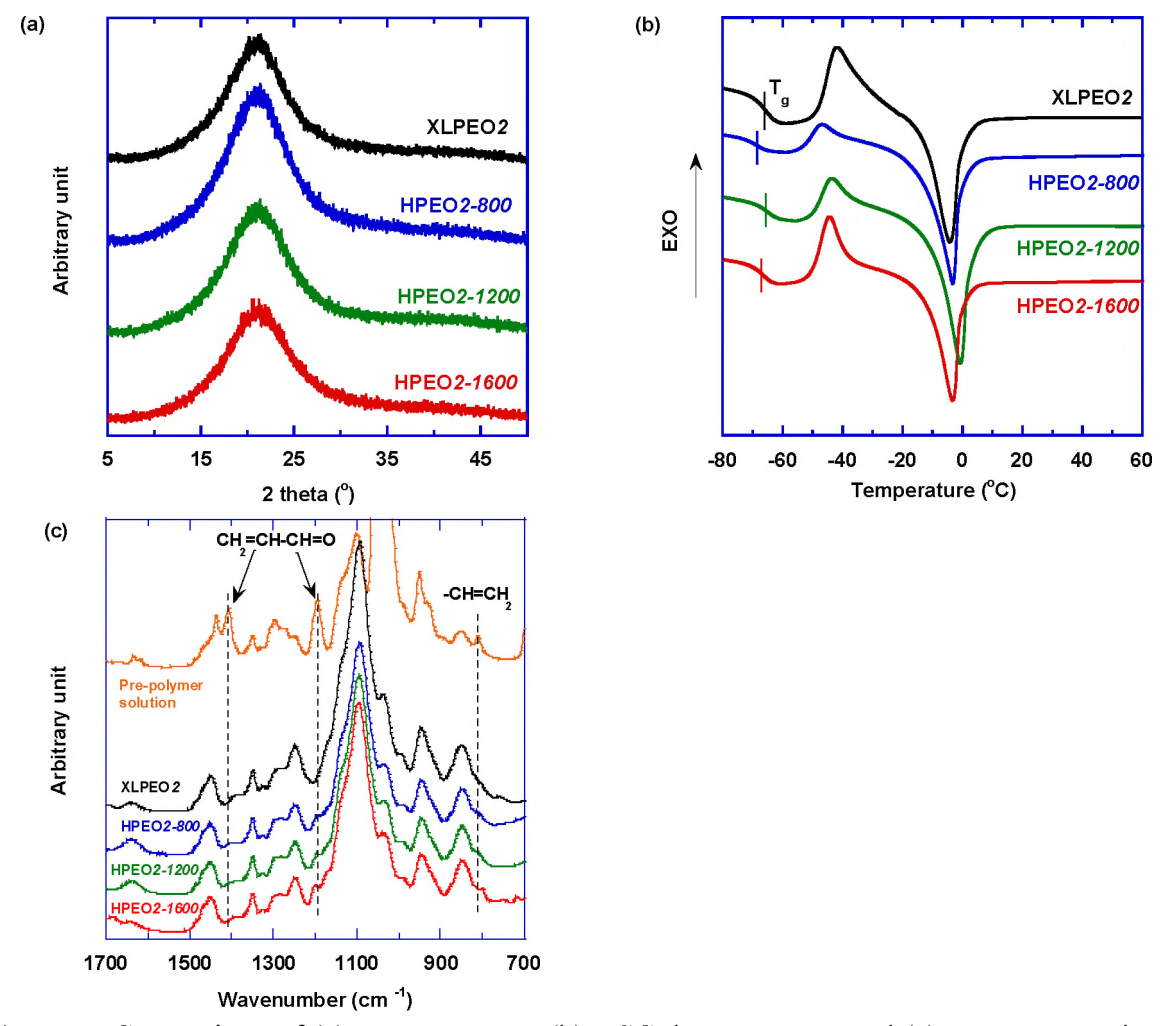


Figure 2. Comparison of (a) XRD patterns, (b) DSC thermograms, and (c) FTIR spectra between HPEO2 and XLPEO2.

Figure 2b compares DSC thermograms of XLPEO2 and HPEO2 films. All polymers exhibit similar thermal transitions (cf. Table 1), including T_g , melting enthalpy (ΔH_m), crystallization temperature (T_c), and melting temperature (T_m). The Mn does not exert a significant effect on the thermal transitions since all polymers have very high Mn values. The DSC thermograms also confirm that the HPEO2 samples are amorphous at ≈ 23 °C. Figure 2c compares FTIR spectra of the HPEO2 and prepolymer solution. The characteristic peaks for the acrylate

groups in the PEGMEA and PEGDA (812, 1190, and 1410 cm⁻¹) almost disappear after the reaction, indicating almost full conversion of the monomers [40].

Table 1. Comparison of physical properties of XLPEO2 and HPEO2 samples.

Properties	XLPEO2	HPEO2-400	HPEO2-800	HPEO2-1200	HPEO2-1600
Mn (kg/mol)	Infinite	142	192	222	198
PDI	N/A	2.1	5.2	5.2	5.4
T_m (°C)	-4.2	-6.3	-3.3	-0.9	-3.4
T_c (°C)	-42	-39	-47	-44	-44
ΔH_m (J/g)	37	37	45	48	44
T_g (°C)	-66	-67	-69	-65	-66
d-spacing (Å)	4.2	N/A	4.2	4.2	4.2
$ ho_P(\mathrm{g/cm^3})$	1.140±0.003	N/A	1.151±0.004	1.131±0.005	1.114±0.008
FFV	0.146	N/A	0.138	0.153	0.166

The density can be used to calculate the fractional free volume (*FFV*) of the polymers using Equation 6:

$$FFV = \frac{V - V_0}{V} \tag{6}$$

where V means the polymer specific volume at the temperature of interest, and V_{θ} is the specific occupied volume at 0 K, which is 1.3 times the van der Waals volume estimated using a group contribution method. Interestingly, the FFV values slightly increase with increasing Mn, presumably caused by the increased PDI and the rich end groups in these hyperbranched polymers [41].

3.2 Pure-gas transport properties of HPEO

Figure 3a shows the pure-gas permeability of N₂, CH₄, H₂, and CO₂ in HPEO2-800. N₂, CH₄, and H₂ show permeability independent of the feed pressure, indicating that the films are defect-free. CO₂ permeability slightly increases from 510 to 540 Barrer with the pressure increasing from 10 to 40 psig because of the plasticization effect of CO₂ [14, 40].



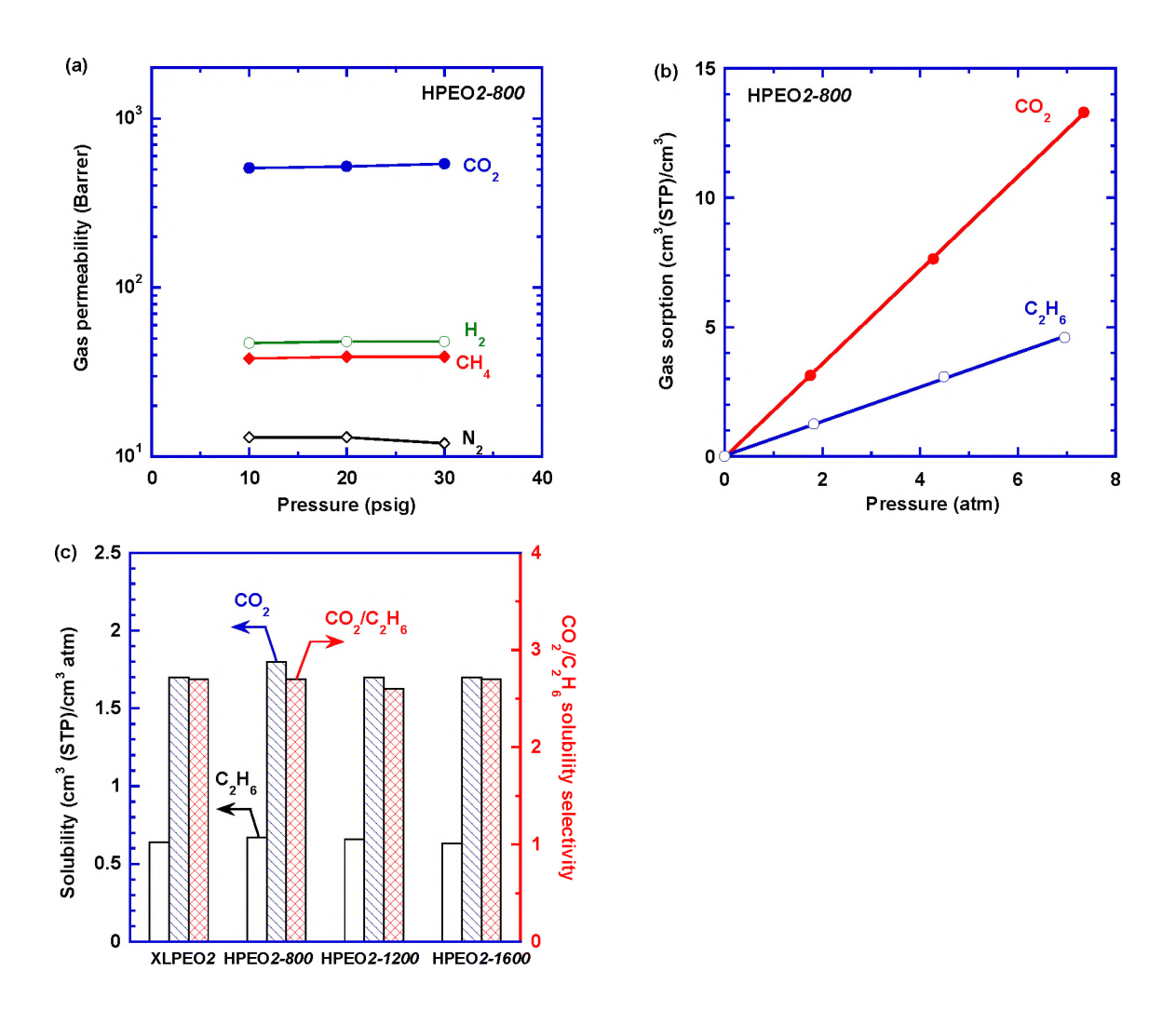


Figure 3. (a) Pure-gas permeability of N_2 , CH_4 , H_2 , and CO_2 in HPEO2-800. (b) Pure-gas sorption isotherms of C_2H_6 and CO_2 in HPEO2-800 at 35°C. (c) Comparison of pure-gas CO_2 solubility and CO_2/C_2H_6 solubility selectivity in XLPEO2 and HPEO2-800.

Table 2 compares the CO₂/gas separation properties for XLPEO₂ and HPEO at 35°C. Increasing the molecular weight decreases the CO₂ permeability from 540 to 450 Barrer while

retaining the CO₂/N₂ selectivity of 45. The polymerization methods (ATRP and photopolymerization) do not significantly influence gas permeability.

Table 2. Comparison of CO₂/gas separation properties of XLPEO₂ and HPEO₂ at 35°C and 30 psig.

D 1	P _{CO2} - (Barrer)	Pure-gas selectivity			S_{CO_2}	$D_{CO_0} \times 10^6$
Polymers		CO ₂ /N ₂	CO ₂ /CH ₄	CO ₂ /H ₂	cm ³ (STP) cm ⁻³ atm ⁻¹)	$D_{CO_2} \times 10^6$ (cm ² s ⁻¹)
XLPEO2	560	47	16	12	1.7	2.5
HPEO2-800	540	43	14	11	1.8	2.3
HPEO2-1200	480	45	15	10	1.7	2.2
HPEO2-1600	450	45	15	12	1.7	2.0

Gas sorption isotherms of CO₂ and C₂H₆ were measured at 35°C. These polymers have the sorption of N₂, CH₄, and H₂ too low to determine accurately using our apparatus. Therefore, C₂H₆ was used as a surrogate, as it does not have specific interactions with the ethylene oxide groups in these polymers [38, 40]. Figure 3b presents the sorption isotherms for C₂H₆ and CO₂ in HPEO2-800, and the isotherms of other polymers are shown in Figure S2. Within the pressure range studied, the gas sorption isotherms are linear, and thus, S_A is calculated and recorded in Table 2. Figure 3c compares CO₂ and C₂H₆ sorption behavior in XLPEO₂ and HPEO₂ at 35°C. All polymers exhibit similar gas solubility coefficients because these polymers have similar chemical compositions, such as the content of the ethylene oxide groups [38]. By contrast, the CO₂ diffusivity slightly decreases with increasing Mn (Table 2), despite the increased *FFV*. This can be partially ascribed to the increased softness with increasing Mn and thus the severer effect of the compaction caused by the feed pressure. However, the mechanical properties of the films were too weak to determine using our rheometer.

3.3 Fabrication and characterization of TFC membranes based on HPEO2-800

The TFC membranes were fabricated using a multi-step coating procedure. First, a gutter layer of PDMS was coated on top of the pretreated PSF support due to its high gas permeability, excellent thin-film forming ability, and thus negligible gas transport resistance [7, 15, 42]. Second, HPEO2-800 with optimal CO₂/N₂ separation properties and mechanical properties was chosen as the selective layer material. The solvent of the coating solutions should have good wettability on the PDMS surface to obtain thin defect-free layers. Figure 4a presents the contact angles of different solvents with various degrees of hydrophilicity on the PDMS surface. IPA has a contact angle of 20°, indicating its excellent compatibility with PDMS, and therefore, it is used as the solvent for HPEO2. Additionally, 3.5 mass% water was added into the coating solutions to improve the solubility of HPEO2.



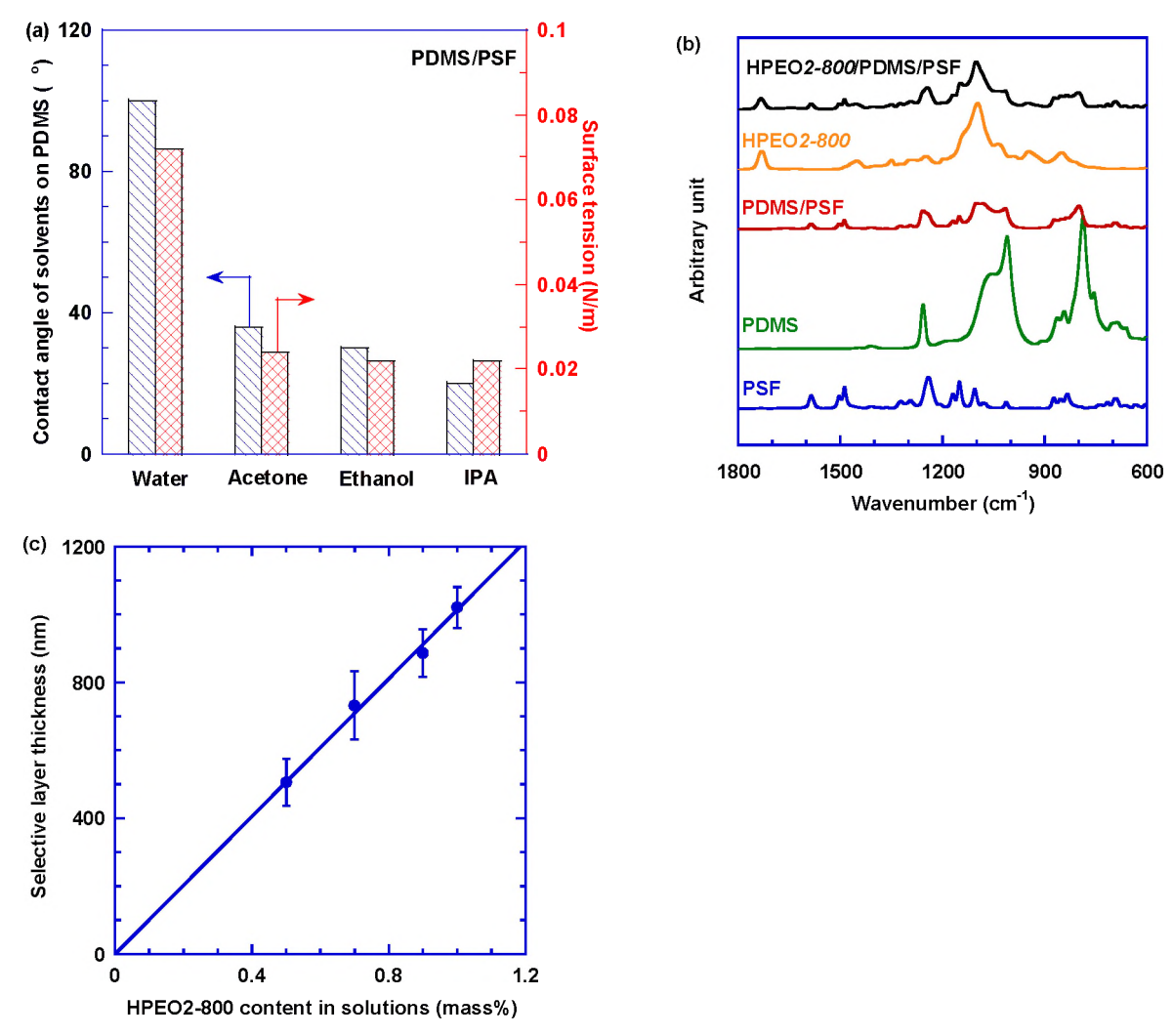


Figure 4. Characterization of TFC membranes. (a) Contact angle of different solvents on the PDMS surface. (b) FTIR spectra of different layers of TFC membranes. (c) Impact of the HPEO2-800 concentration on the selective layer thickness (cf. Table S2).

Figure 4b shows FTIR spectra of different coating layers. After coating the HPEO2 on the PDMS layer, the characteristic peak of the ethylene oxide (1100 cm $^{-1}$) appears, confirming the successful coating of the HPEO2. Figure 4c demonstrates that increasing the HPEO2 content in the coating solutions increases its layer thickness. The thinnest defect-free selective layer (506 \pm 44 nm) was fabricated using a 0.5 mass% coating solution.

Figure 5a,b shows the cross-sectional SEM image of the PDMS/PSF and HPEO2-800/PDMS/PSF, respectively. The PDMS and HPEO2-800 layer has a thickness of ≈150 and ≈480 nm, respectively, which are consistent with the F20 measurement results (PDMS: 145±50 nm, and HPEO: 506±44 nm). The PDMS gutter layer surface is smoothed out with an average roughness of 4.7 nm (Figure 5c). The average surface modulus is taken from the modulus map and has a value of 11 MPa (Figure 5e). It is stiffer than the bulk PDMS because of the substrate effect since the coating is so thin [43]. When HPEO2-800 is coated on the PDMS, the texture does not change much but still further smooths out, and the average roughness falls to 3.7 nm (Figure 5d). The amorphous HPEO appears to be very sticky, as noted by the increase in adhesion from an average of 12 to 75 nN (Figure 5g,h), and it does not behave elastically. Because of this, quantification of the surface modulus (Figure 5f) is unreliable. Nevertheless, the PDMS and HPEO/PDMS do show distinct surface property differences, confirming the successful coating of PDMS and HPEO.

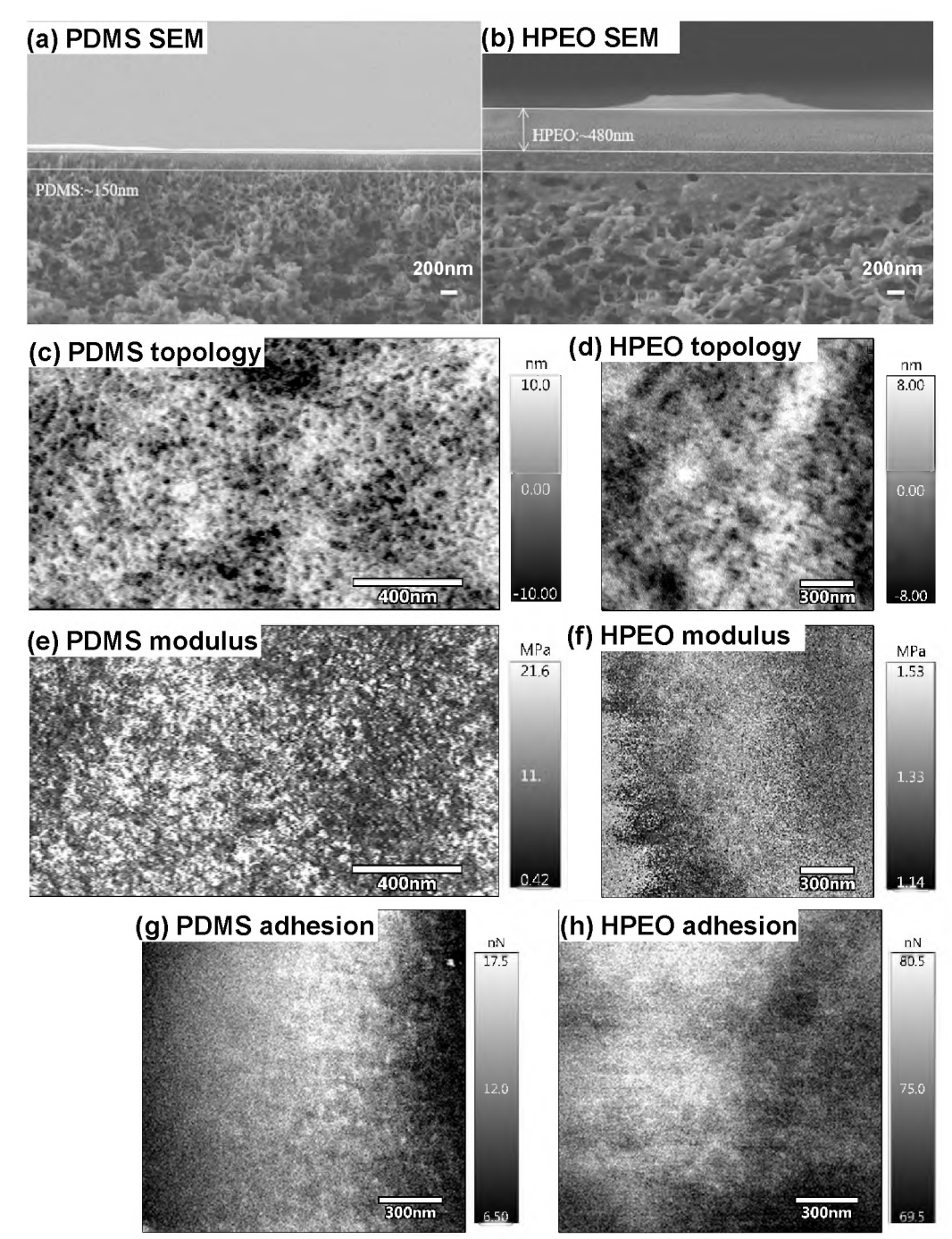


Figure 5. Comparison of the PDMS/PSF and HPEO2/PDMS/PSF membranes. Cross-sectional SEM photos of (a) PDMS and (b) HPEO2. AFM topography map of (c) PDMS and (d) HPEO2. Modules map of (e) PDMS and (f) HPEO2. Adhesion scans of (g) PDMS and (h) HPEO2.

The PDMS/PSF displays CO₂ permeance of 10,000 GPU and CO₂/N₂ selectivity of 10 at 35°C. While the selectivity is consistent with the literature (indicating that the PDMS layer is

defect-free), the CO₂ permeance is much lower than expected (25,000 GPU based on the CO₂ permeability of 3800 Barrer and the thickness of 150 nm) [44], which can be ascribed to the geometric restriction by the surface pore size and porosity of the PSF support [34, 45, 46].

 Figure 6a presents the influence of the selective layer thickness on CO_2 permeance and CO_2/N_2 selectivity of the TFC membranes at 35°C. As expected, increasing the selective layer thickness decreases gas permeance $((P/l)_M)$ and increases CO_2/N_2 selectivity, which is caused by the gutter layer with low selectivity and non-negligible gas transport resistance. Gas permeance can be described using the resistance-in-series model:

$$\left(\frac{l}{p}\right)_{M} = \left(\frac{l}{p}\right)_{HPEO} + \left(\frac{l}{p}\right)_{PDMS} \tag{7}$$

where $(l/P)_{HPEO}$ and $(l/P)_{PDMS}$ are the gas transport resistance (or the inverse of gas permeance) of the HPEO and PDMS layer, respectively. The resistance of the PSF support is negligible because of its extremely high gas permeance (such as 800,000 GPU for CO₂).

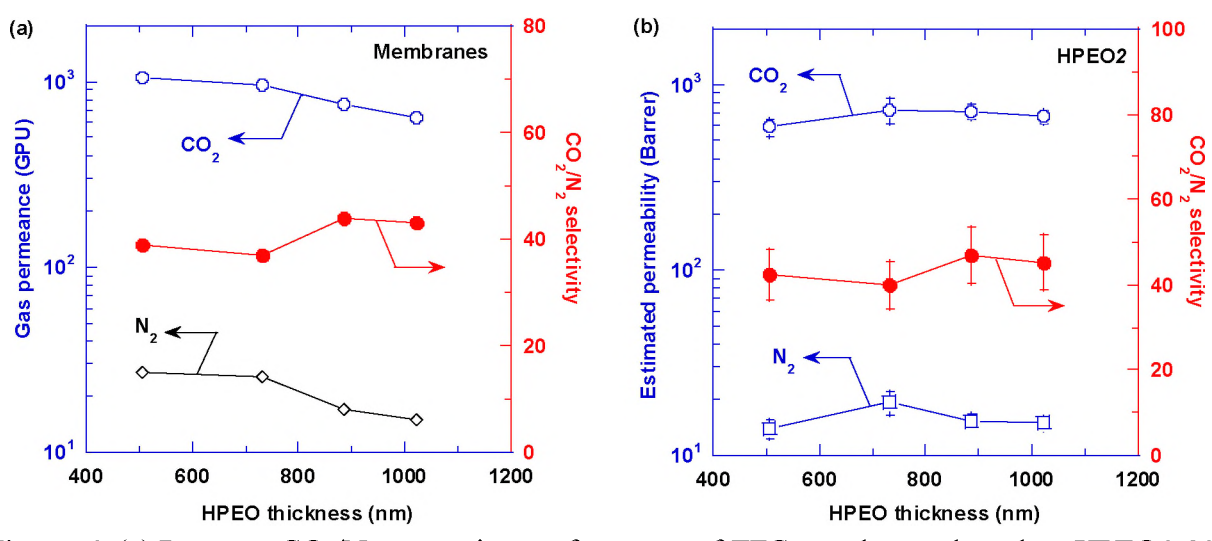
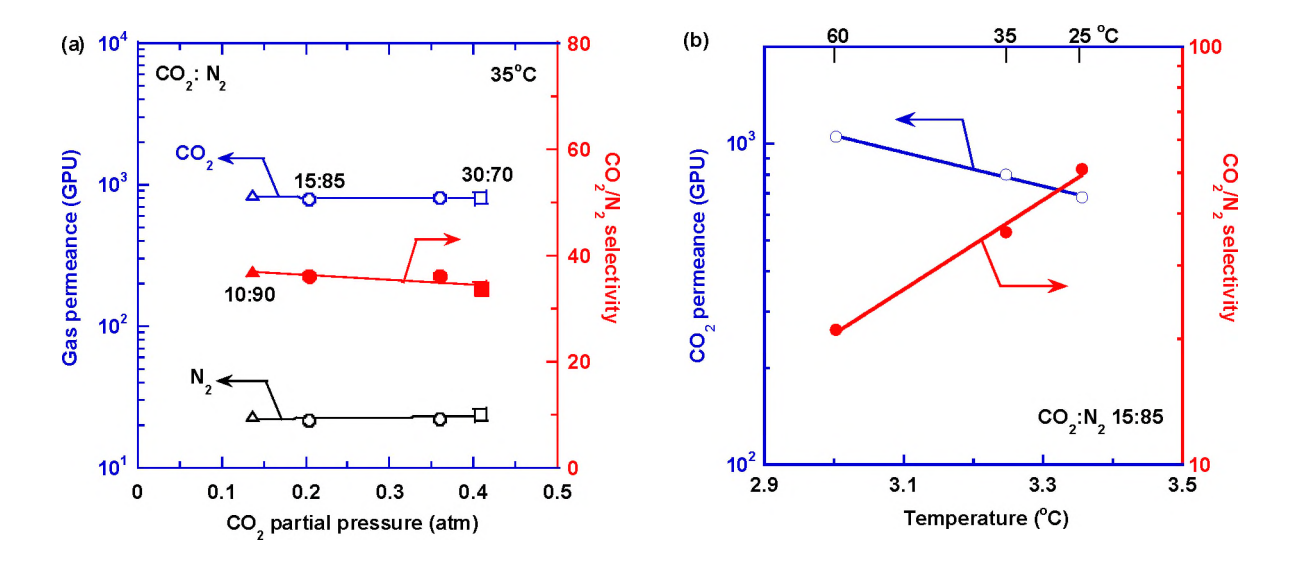


Figure 6. (a) Pure-gas CO₂/N₂ separation performance of TFC membranes based on HPEO2-800 at 35°C. (b) Estimated CO₂/N₂ separation performance of the HPEO2-800 selective layer based on Equation 7.

Figure 6b presents the calculated permeability and selectivity for the HPEO selective layer by Equation 7. As expected, the HPEO2 layer of the membranes exhibits similar CO_2/N_2 separation properties, which are also close to those of the freestanding films of HPEO2.

3.4 CO₂/N₂ separation performance of TFC membranes

The membrane containing 506-nm HPEO2-800 exhibits optimal CO₂ permeance and CO₂/N₂ selectivity, and thus it was thoroughly evaluated with gas mixtures at different temperatures for typical flue gas streams. Figure 7a shows the influence of CO₂ partial pressure on the mixed-gas permeance at 35°C. Two mixtures of CO₂:N₂ (10:90 and 30:70) were used at a feed pressure of 1.4 atm, and the third mixture of CO₂:N₂ (15:85) was tested at 1.4 and 2.1 atm. Increasing the feed CO₂ pressure has a negligible impact on CO₂ permeance and CO₂/N₂ selectivity because of the low CO₂ partial pressure and thus insignificant effect of plasticization.



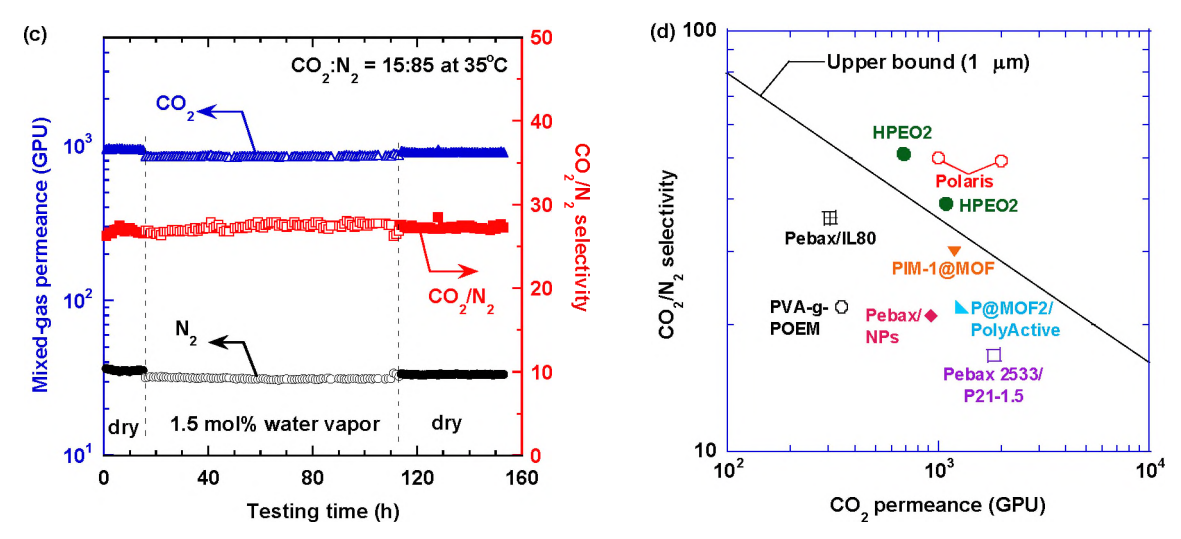


Figure 7. Excellent mixed-gas CO₂/N₂ separation performance in HPEO*2-800*/PDMS/PSF. Influence of (a) CO₂ partial pressure and (b) temperature on CO₂/N₂ separation properties. The curves in (b) are based on Equation 8. (c) Separation performance when tested with CO₂/N₂ (15:85) and 1.5 mol% water vapor at 2 atm and 35°C. (d) Comparison of HPEO₂ with state-of-the-art membranes for CO₂/N₂ separation, including Polaris [4], Pebax 2533/P21-1.5 [47], PIM-1@MOF [48], PVA-g-POEM [49], Pebax/IL80 [50], Pebax/NPs [51], and P@MOF2/PolyActive [52]. The upper bound is drawn, assuming that all the materials are fabricated into 1-μm selective layer. Details of these membranes are provided in Table S3.

Figure 7b presents the mixed-gas CO₂/N₂ separation properties at 25 - 60°C with a gas mixture of CO₂/N₂ (15:85), typical flue gas from coal-fired power plants. Decreasing the temperature decreases mixed-gas permeance and increases CO₂/N₂ selectivity, consistent with the behaviors of freestanding films [14]. For example, decreasing the temperature from 60 to 25°C decreases CO₂ permeance from 1050 to 680 GPU and increases CO₂/N₂ selectivity from 20 to 50. Lowering temperature reduces the polymer chain mobility and thus gas diffusivity and increases CO₂/N₂ solubility selectivity due to the enhanced affinity of the polymer towards CO₂. The effect of the temperature on gas permeability can be described using Arrhenius Equation [14]:

379
$$P_A = P_{A,0} \exp(-\frac{E_{P,A}}{RT})$$
 (8)

where $P_{A,0}$ is a front factor (Barrer), and $E_{P,A}$ is the activation energy of permeation (kJ/mol). The best fittings in Figure 7b yields the and $E_{P,A}$ value of 10 kJ/mol for CO₂, which is lower than N₂

(30 kJ/mol), consistent with the smaller kinetic diameter of CO₂ than N₂ and the literature [14]. As such, decreasing the temperature increases the CO₂/N₂ selectivity.

Flue gas often contains water vapor, which can be absorbed by the HPEO due to its hydrophilicity. Figure 7c presents the impact of the water vapor on the CO₂/N₂ separation properties. The membrane was initially exposed to CO₂/N₂ (15:85) at 2 barg and 35°C for 15 h. When 1.5 mol% water vapor was added to the feed, CO₂ permeance decreases from 950 to 850 GPU, and N₂ permeance decreases from 36 to 32 GPU while the CO₂/N₂ selectivity remains at ≈27, presumably because of the increased selective layer thickness by water absorption, consistent with those in PEO [6, 39]. However, our apparatus does not allow us to monitor in situ the thickness of the selective layer in this multi-layer membrane. Though the real flue gas contains water vapor content higher than 1.5 mol%, the result indicates that the HPEO membrane shows stable separation performance with water vapor in 98 h. When tested again with the dry mixture, the CO₂/N₂ separation properties recover to the initial values, indicating the membrane stability. The membranes should be systematically tested with simulated flue gas containing higher water vapor pressure and real flue gas for long-term stability. However, it is beyond the scope of this study.

Figure 7d compares the HPEO2-800 with Robeson's upper bound for CO₂/N₂ separation, assuming that all polymers can be fabricated into membranes with 1-μm selective layer. The HPEO2-800 membrane has pure-gas CO₂ permeance of 1000 GPU and CO₂/N₂ selectivity of 39 at 35°C, surpassing the upper bound and superior to Pebax 2533/P21-4.3 with CO₂ permeance of 1330 GPU and CO₂/N₂ selectivity of 18 [47], and PIM-1@MOF with CO₂ permeance of 1200 GPU and CO₂/N₂ selectivity of 30 [48]. The HPEO2-800 membranes show CO₂/N₂ selectivity of 51 at ≈ 23°C, comparable with a commercial membrane, PolarisTM [4]. In summary, the HPEO2-

800 based membranes meet the requirement of the membranes for post-combustion carbon capture (CO₂ permeance of 1000 GPU and CO₂/N₂ selectivity of 30), and the performance can be improved by lowering the thickness of the selective layer and the transport resistance of the gutter layer.

408

409

410

411

412

413

414

415

416

417

418

419

420

421

422

423

424

405

406

407

4. Conclusions

We demonstrate that soluble, amorphous, and high molecular weight PEO can be synthesized from acrylate-based monomers using ATRP and then fabricated into highperformance TFC membranes for post-combustion carbon capture. A series of HPEO0 and HPEO2 with various molecular weight values were successfully synthesized. The HPEO2 shows better mechanical properties than HPEO0, and thus, HPEO2 is further investigated for gas transport properties. Compared with XLPEO2 prepared from photopolymerization, HPEO2 exhibits similar thermal transitions, free volume, and pure-gas transport properties. HPEO2-800 with CO₂ permeability of 540 Barrer and CO₂/N₂ selectivity of 43 was selected to fabricate TFC membranes. When challenged with simulated flue gas containing 1.5 mol% H₂O for 100 h, the membrane shows stable mixed-gas CO₂ permeance of 850 GPU and CO₂/N₂ selectivity of 37 at 35°C, which is close to the upper bound and comparable with the leading industrial membranes, demonstrating their potential for practical applications. The membranes will be tested with real flue gas for longterm stability to move the technology beyond the laboratory. This work reveals a new route of preparing TFC membranes using state-of-the-art industrial manufacturing processes from conventional cross-linked polymers.

425

426

Acknowledgments

- We gratefully acknowledge the financial support from the United States Department of
- 428 Energy (DE-FE0031736) and the National Science Foundation (1554236).

430

References

- Y. Han, W. S. Ho. Polymeric membranes for CO₂ separation and capture. J. Membr. Sci. 628 (2021) 119244.
- T. C. Merkel, H. Lin, X. Wei, R. W. Baker. Power plant post-combustion carbon dioxide capture: An opportunity for membranes. J. Membr. Sci. 359 (2010) 126-139.
- H. Park, J. Kamcev, L. M. Robeson, M. Elimelech, B. D. Freeman. Maximizing the right stuff: The trade-off between membrane permeability and selectivity. Science. 356 (2017) eaab0530.
- 438 [4] L. S. White, K. D. Amo, T. Wu, T. C. Merkel. Extended field trials of Polaris sweep modules for carbon capture. J. Membr. Sci. 542 (2017) 217-225.
- Z. Qiao, S. Zhao, M. Sheng, J. Wang, S. Wang, Z. Wang, C. Zhong, M. D. Guiver.
 Metal-induced ordered microporous polymers for fabricating large-area gas separation membranes. Nat. Mater. 18 (2019) 163-168.
- J. Liu, S. Zhang, D. Jiang, C. M. Doherty, A. J. Hill, C. Cheng, H. B. Park, H. Lin. Highly Polar but Amorphous Polymers with Robust Membrane CO₂/N₂ Separation Performance. Joule. 3 (2019) 1881-1894.
- M. Galizia, W. S. Chi, Z. P. Smith, T. C. Merkel, R. W. Baker, B. D. Freeman. 50th anniversary perspective: polymers and mixed matrix membranes for gas and vapor separation: a review and prospective opportunities. Macromolecules. 50 (2017) 7809-7843.
- M. Barooah, B. Mandal, B. Su. Enhanced CO₂ separation performance of mixed matrix membrane by incorporating amine functionalized silica filler. J. Appl. Polym. Sci. 138 (2021) 51438.
- J. Liu, X. Hou, H. B. Park, H. Lin. High-performance polymers for membrane CO₂/N₂ Separation. Chem. Eur. J. 22 (2016) 15980-15990.
- B. Zhu, X. Jiang, S. He, X. Yang, J. Long, Y. Zhang, L. Shao. Rational design of poly(ethylene oxide) based membranes for sustainable CO₂ capture. J. Mater. Chem. A. 8 (2020) 24233-24252.
- H. Lin, B. D. Freeman. Materials selection guidelines for membranes that remove CO₂ from gas mixtures. J. Mol. Struct. 739 (2005) 57-74.
- 460 [12] X. Jiang, S. Li, L. Shao. Pushing CO₂-philic membrane performance to the limit by 461 designing semi-interpenetrating networks (SIPN) for sustainable CO₂ separations. Energy 462 Environ. Sci. 10 (2017) 1339-1344.
- C. G. Rodriguez, M. Chwatko, J. Park, C. L. Bentley, B. D. Freeman, N. A. Lynd.
 Compositionally controlled polyether membranes via mono(mualkoxo)bis(alkylaluminum)-Initiated chain-growth network epoxide polymerization:
 synthesis and transport properties. Macromolecules. 53 (2020) 1191-1198.

- H. Lin, E. Van Wagner, J. S. Swinnea, B. D. Freeman, S. J. Pas, A. J. Hill, S.
 Kalakkunnath, D. S. Kalika. Transport and structural characteristics of crosslinked poly
 (ethylene oxide) rubbers. J. Membr. Sci. 276 (2006) 145-161.
- H. Lin, Z. He, Z. Sun, J. Vu, A. Ng, M. Mohammad, J. Kniep, T. C. Merkel, T. Wu, R. C.
 Lambrecht. CO₂-selective membranes for hydrogen production and CO₂ capture Part I:
 Membrane development. J. Membr. Sci. 457 (2014) 149-161.
- 473 [16] M. Liu, M. D. Nothling, P. A. Webley, Q. Fu, G. G. Qiao. Postcombustion carbon capture using thin-film composite membranes. Acc. Chem. Res. 52 (2019) 1905-1914.
- S. J. Metz, M. H. V. Mulder, M. Wessling. Gas-permeation properties of poly(ethylene oxide) poly(butylene terephthalate) block copolymers. Macromolecules. 37 (2004) 4590-4597.
- V. I. Bondar, B. D. Freeman, I. Pinnau. Gas transport properties of poly(ether-*b*-amide) segmented block copolymers. J. Polym. Sci.: Part B: Polym. Phys. 38 (2000) 2051-2062.
- 480 [19] A. Car, C. Stropnik, W. Yave, K. V. Peinemann. Tailor-made Polymeric Membranes 481 based on Segmented Block Copolymers for CO₂ Separation. Adv. Funct. Mater. 18 482 (2008) 2815-2823.
- 483 [20] T. Li, Y. Pan, K.-V. Peinemann, Z. Lai. Carbon dioxide selective mixed matrix 484 composite membrane containing ZIF-7 nano-fillers. J. Membr. Sci. 425-426 (2013) 235-485 242.
- W. Yave, H. Huth, A. Car, C. Schick. Peculiarity of a CO₂-philic block copolymer confined in thin films with constrained thickness: "a super membrane for CO₂-capture". Energy Environ. Sci. 4 (2011) 4656-4661.
- W. Yave, A. Car, J. Wind, K. Peinemann. Nanometric thin film membranes manufactured on square meter scale: Ultra-thin films for CO₂ capture. Nanotechnology. 21 (2010) 1-7.
- 492 [23] Q. Fu, J. Kim, P. A. Gurr, J. M. Scofield, S. E. Kentish, G. G. Qiao. A novel cross-linked nano-coating for carbon dioxide capture. Energy Environ. Sci. 9 (2016) 434-440.
- 494 [24] M. Liu, K. Xie, M. D. Nothling, L. Zu, S. Zhao, D. J. Harvie, Q. Fu, P. A. Webley, G. G.
 495 Qiao. Ultrapermeable composite membranes enhanced via doping with amorphous MOF
 496 nanosheets. ACS Cent. Sci. 7 (2021) 671-680.
- 497 [25] T. Zhao, H. Zhang, D. Zhou, Y. Gao, Y. Dong, U. Greiser, H. Tai, W. Wang. Water 498 soluble hyperbranched polymers from controlled radical homopolymerization of PEG 499 diacrylate. RSC Adv. 5 (2015) 33823-33830.
- 500 [26] K. Matyjaszewski. Atom transfer radical polymerization (ATRP): Current status and future perspectives. Macromolecules. 45 (2012) 4015-4039.
- [27] H. Zhang, T. Zhao, P. Duffy, Y. Dong, A. N. Annaidh, E. O'Cearbhaill, W. Wang.
 Hydrolytically Degradable Hyperbranched PEG Polyester Adhesive with Low Swelling
 and Robust Mechanical Properties. Adv. Healthc. Mater. 4 (2015) 2260-2268.
- 505 [28] S. Zhai, J. Shang, D. Yang, S. Wang, J. Hu, G. Lu, X. Huang. Successive SET LRP and ATRP synthesis of ferrocene based PPEGMEA g PAEFC well defined amphiphilic graft copolymer. J. Polym. Sci. A: Polym. Chem. 50 (2012) 811-820.
- J. Miao, W. He, L. Zhang, Y. Wang, Z. Cheng, X. Zhu. AGET ATRP of water-soluble
 PEGMA: Fast living radical polymerization mediated by iron catalyst. J. Polym. Sci. Part
 A: Polym. Chem. 50 (2012) 2194-2200.

- [30] K. Matyjaszewski, N. V. Tsarevsky, W. A. Braunecker, H. Dong, J. Huang, W.
 Jakubowski, Y. Kwak, R. Nicolay, W. Tang, J. Yoon. Role of Cu0 in
 Controlled/"Living" Radical Polymerization. Macromolecules. 40 (2007) 7795-7806.
- [31] F. Alsubaie, A. Anastasaki, V. Nikolaou, A. Simula, G. Nurumbetov, P. Wilson, K.
 Kempe, D. M. Haddleton. Investigating the Mechanism of Copper(0)-Mediated Living
 Radical Polymerization in Aqueous Media. Macromolecules. 48 (2015) 6421-6432.
- J. Liu, C. R. P. Fulong, L. Hu, L. Huang, G. Zhang, T. R. Cook, H. Lin. Interpenetrating networks of mixed matrix materials comprising metal-organic polyhedra for membrane CO₂ capture. J. Membr. Sci. 606 (2020) 118122.
- 520 [33] J. Liu, G. Zhang, K. Clark, H. Lin. Maximizing ether oxygen content in polymers for 521 membrane CO₂ removal from natural gas. ACS Appl. Mater. Interfaces. 11 (2019) 522 10933-10940.
- 523 [34] L. Zhu, W. Jia, M. Kattula, K. Ponnuru, E. P. Furlani, H. Lin. Effect of porous supports 524 on the permeance of thin film composite membranes: Part I. Track-etched polycarbonate 525 supports. J. Membr. Sci. 514 (2016) 684-695.
- [35] J. S. Velázquez-González, D. Monzón-Hernández, D. Moreno-Hernández, F. Martínez Piñón, I. Hernández-Romano. Simultaneous measurement of refractive index and
 temperature using a SPR-based fiber optic sensor. Sens. Actuators B Chem. 242 (2017)
 912-920.
- [36] W. Ogieglo, H. Wormeester, M. Wessling, N. E. Benes. Spectroscopic ellipsometry
 analysis of a thin film composite membrane consisting of polysulfone on a porous α-alumina support. ACS Appl. Mater. Interfaces. 4 (2012) 935-943.
- 533 [37] M. Choi, M. Humar, S. Kim, S. H. Yun. Step index optical fiber made of biocompatible hydrogels. Adv. Mater. 27 (2015) 4081-4086.
- H. Lin, B. D. Freeman. Gas solubility, diffusivity and permeability in poly(ethylene oxide). J. Membr. Sci. 239 (2004) 105-117.
- 537 [39] L. Huang, J. Liu, H. Lin. Thermally stable, homogeneous blends of cross-linked poly 538 (ethylene oxide) and crown ethers with enhanced CO₂ permeability. J. Membr. Sci. 610 539 (2020) 118253.
- 540 [40] H. Lin, B. D. Freeman. Gas permeation and diffusion in cross-linked poly(ethylene glycol diacrylate). Macromolecules. 39 (2006) 3568-3580.
- [41] E. Langer, K. Bortel, S. Waskiewicz, M. Lenartowicz-Klik. 1 Assessment of Traditional
 Plasticizers. In: Langer E, Bortel K, Waskiewicz S, Lenartowicz-Klik M, editors.
 Plasticizers Derived from Post-Consumer PET: William Andrew Publishing; 2020. p. 1 11.
- 546 [42] M. Kattula, K. Ponnuru, L. Zhu, W. Jia, H. Lin, E. P. Furlani. Designing ultrathin film composite membranes: The impact of a gutter layer. Sci. Rep. 5 (2015) 15016.
- [43] L. Zhu, L. Huang, S. R. Venna, A. K. Blevins, Y. Ding, D. P. Hopkinson, M. T. Swihart,
 H. Lin. Scalable Polymeric Few-Nanometer Organosilica Membranes with Hydrothermal
 Stability for Selective Hydrogen. ACS Nano. 15 (2021) 12119-12128.
- T. C. Merkel, V. I. Bondar, K. Nagai, B. D. Freeman, I. Pinnau. Gas sorption, diffusion,
 and permeation in poly (dimethylsiloxane). J. Polym. Sci. Part B: Polym. Phys. 38 (2000)
 415-434.
- J. G. Wijmans, P. Hao. Influence of the porous support on diffusion in composite membranes. J. Membr. Sci. 494 (2015) 78-85.

- L. Zhu, M. Yavari, W. Jia, E. P. Furlani, H. Lin. Geometric Restriction of Gas Permeance in Ultrathin Film Composite Membranes Evaluated Using an Integrated Experimental and Modeling Approach. Industrial & Engineering Chemistry Research. 56 (2017) 351-358.
- J. M. Scofield, P. A. Gurr, J. Kim, Q. Fu, S. E. Kentish, G. G. Qiao. Development of novel fluorinated additives for high performance CO₂ separation thin-film composite membranes. J. Membr. Sci. 499 (2016) 191-200.
- 563 [48] M. Liu, M. D. Nothling, P. A. Webley, J. Jin, Q. Fu, G. G. Qiao. High-throughput CO₂ capture using PIM-1@ MOF based thin film composite membranes. Chem. Eng. J. 396 (2020) 125328.
- 566 [49] M. Park, Y. Choi, K. Lee, J. Kim. Synthesis of PVA-g-POEM graft copolymers and their use in highly permeable thin film composite membranes. Chem. Eng. J. 346 (2018) 739-747.
- 569 [50] W. Fam, J. Mansouri, H. Li, V. Chen. Improving CO₂ separation performance of thin film composite hollow fiber with Pebax® 1657/ionic liquid gel membranes. J. Membr. Sci. 537 (2017) 54-68.
- 572 [51] Q. Fu, E. Wong, J. Kim. The effect of soft nanoparticles morphologies on thin film composite membrane performance. J. Mater. Chem. A. 2 (2014) 17751-17756.
- 574 [52] K. Xie, Q. Fu, J. Kim, H. Lu, Y. He, Q. Zhao, J. Scofield, P. A. Webley, G. G. Qiao.
 575 Increasing both selectivity and permeability of mixed-matrix membranes: Sealing the
 576 external surface of porous MOF nanoparticles. J. Membr. Sci. 535 (2017) 350-356.